Journal of the American College of Cardiology
© 2006 by the American College of Cardiology Foundation
Published by Elsevier Inc.

Vol. 48, No. 10, 2006
ISSN 0735-1097/06/$32.00
doi:10.1016/j.jacc.2006.08.019

FOCUS ISSUE: CARDIAC IMAGING

Single-Beat Noninvasive Imaging of Cardiac Electrophysiology of Ventricular Pre-Excitation

Thomas Berger, MD,* Gerald Fischer, PHD,‡ Bernhard Pfeifer, PHD,‡ Robert Modre, PHD,‡ Friedrich Hanser, PHD,‡ Thomas Trieb, MD,† Franz X. Roithinger, MD,* Markus Stuehlinger, MD,* Otmar Pachinger, MD,* Bernhard Tilg, PHD,‡ Florian Hintringer, MD*

Innsbruck and Hall, Austria

OBJECTIVES The aim of this study was to determine whether noninvasive imaging of cardiac electrophysiology (NICE) is feasible in patients with Wolff-Parkinson-White (WPW) syndrome in the clinical setting of a catheter laboratory and to test the accuracy of the noninvasively obtained ventricular activation sequences as compared with that of standard invasive electroanatomic mapping.

BACKGROUND NICE of ventricular activation could serve as a useful tool in the treatment of cardiac arrhythmias and might help improve our understanding of arrhythmia mechanisms.

METHODS NICE works by fusing the data from high-resolution electrocardiographic mapping and a model of the patient's cardiac anatomy obtained by magnetic resonance imaging. The ventricular activation sequence was computed with a bidomain theory-based heart model to solve this inverse problem. Noninvasive imaging of cardiac electrophysiology was performed in 7 patients with WPW syndrome undergoing catheter ablation of the accessory pathway. The position error of NICE was defined as the distance between the site of earliest activation computed by NICE and the successful ablation site identified by electroanatomic mapping (CARTO; Biosense Webster, Diamond Bar, California) for normal atrioventricular (AV) conduction as well as for adenosine-induced AV block.

RESULTS The error introduced by geometric coupling of the CARTO data and the NICE model was 5 ± 3 mm (model discretization 10 mm). All ventricular accessory pathway insertion sites were identified with an accuracy of 18.7 ± 5.8 mm (baseline) and 18.7 ± 6.4 mm (adenosine).

CONCLUSIONS The individual cardiac anatomy model obtained for each patient enables accurate noninvasive electrocardiographic imaging of ventricular pre-excitation in patients with WPW syndrome. Noninvasive imaging of cardiac electrophysiology might be used as a complementary noninvasive approach to localize the origin and help identify and understand the underlying mechanisms of cardiac arrhythmias. (J Am Coll Cardiol 2006;48:2045–52) © 2006 by the American College of Cardiology Foundation

Radiofrequency catheter ablation procedures have demonstrated major progress in the treatment of cardiac arrhythmias over the past decade. There are several novel strategies for electrophysiologic mapping and real-time navigation in the 3-dimensional (3D) anatomy of the heart (1,2). Noninvasive techniques, such as computed tomography (CT) or magnetic resonance imaging (MRI), have recently emerged in clinical routine. However, the diagnosis and treatment of many cardiac arrhythmias remains the domain of invasive electrophysiological studies and therefore are dependent on fluoroscopy.

New cardiac imaging techniques, such as the noninvasive imaging of cardiac electrophysiology (NICE) (3–6), are a means of integrating anatomical and electrophysiologic information by coupling noninvasive beat-to-beat analysis of cardiac activation and patient cardiac anatomy. Noninvasive imaging of cardiac electrophysiology might improve our understanding of the underlying arrhythmia mechanisms, even before and during invasive catheter ablation. It might also facilitate localization and ablation of the underlying arrhythmogenic substrate and therefore decrease catheter ablation and fluoroscopy time.

The aim of the present study was to test the hypothesis that noninvasive ventricular activation mapping is feasible in the clinical setting of a catheter laboratory with sufficient spatial and temporal resolution. For the first time, noninvasive mapping of human ventricular pre-excitation was performed and the results were validated by invasive 3D electroanatomic mapping (CARTO; Biosense Webster, Diamond Bar, California).

METHODS

Patient population. Seven patients (3 female; mean age 29 ± 9 years) with overt ventricular pre-excitation under-

From the *Department of Internal Medicine, Division of Cardiology, and †Department of Radiology, Medical University Innsbruck, Innsbruck, Austria; and the ‡Institute for Biomedical Engineering, University for Health Sciences, Medical Informatics, and Technology, Tirol, Austria. This study was supported by the Austrian Science Fund (Fonds zur Förderung der wissenschaftlichen Forschung [FWF]), Grant START Y144, and by Oesterreichische Nationalbank Jubiläumsfond (Jubiläumsfondsprojekt Nr. 11183).

Manuscript received March 1, 2006; revised manuscript received May 16, 2006, accepted May 22, 2006.

JACC Vol. 48, No. 10, 2006
November 21, 2006:2045–52

Abbreviations and Acronyms

AV = atrioventricular
CT = computed tomography
ECG = electrocardiogram/electrocardiography
MRI = magnetic resonance imaging
NICE = noninvasive imaging of cardiac electrophysiology
rms = root mean square
WPW = Wolff-Parkinson-White syndrome

went electrophysiologic examination and subsequent radiofrequency catheter ablation of the accessory pathway. All patients had structurally normal hearts as assessed by prior transthoracic echocardiography. None of the patients were receiving antiarrhythmic drug therapy. Patient characteristics are given in Table 1. The study was approved by the local ethics committee, and written informed consent was obtained from all patients.

MRI. Before electrophysiologic examination, patient-specific anatomical data were obtained by MRI with a Magnetom Vision Plus 1.5-T scanner (Siemens, Erlangen, Germany). The MRI was performed during the morning clinical routine, whereas the electrophysiologic examination was performed in the afternoon with a mean delay of about 2.5 h. Ventricular end-diastolic geometry and torso geometry were assessed in electrocardiogram (ECG)-gated cine mode during breath hold as previously described (3,7). Liquid-filled anatomical markers (vitamin E capsules) on the patient's torso were used to couple the MRI geometric data with the data obtained during electrophysiologic examination.

ECG mapping. A high-resolution 65-lead electrode array was applied in the catheter laboratory before the ablation procedure. Radiotranslucent carbon electrodes were used to facilitate simultaneous fluoroscopy. The ECG recordings were performed with the Mark-8 system (Biosemi V.O.F., Amsterdam, the Netherlands) at a sampling rate of 2,048 Hz (0.3 Hz to 400 Hz band pass filter) and an alternating current (AC) resolution of 500 nV/bit (16 bit analog-to-digital converter, [i.e., 32 mV AC input range]). The Mark-8 is a battery-powered (6 V) high-precision ECG amplifier. It was fixed at bedside to keep wire connections as short as possible. Data were transferred to the recording personal computer via an optic fiber.

Anatomical coupling. As anatomical data were recorded in the MRI frame, all other geometric data also had to be transformed in this frame. For this purpose 7 anterior and lateral MRI markers and the anterior and lateral electrode positions were measured with a magnetic digitizer (Fastrak; Polhemus Inc., Colchester, Vermont). The electrode positions were transformed by a rigid body transformation (rotation matrix and displacement vector), minimizing the root mean square (rms) distance of the 7 Polhemus marker positions to the MRI marker positions. The posterior electrodes were directly applied at the location of the posterior markers. Intra-cardiac data were transformed in the MRI frame with the 7 MRI marker locations with the CARTO (Biosense Webster) catheter (see following text) after the electrophysiologic examination.

NICE. Noninvasive imaging of cardiac electrophysiology requires assessment of the patient's anatomy (MRI) to construct a patient-specific computer model and a high-resolution ECG map providing functional information on target beats (Fig. 1). For each patient a personal computer model, including compartments of different conductivity (heart, lungs, blood mass, and chest surface), was constructed. For this purpose, a commercial software package (AMIRA Developer; TGS Template Graphics Software, Inc., Merignac, France) was adapted for contour detection and segmentation as previously described (3,8).

A bidomain model-based boundary element formulation (linear triangular elements) was applied to relate step-like local activation (resting potential, −90 mV; plateau level, 0 mV; rising time, 3 ms) at the endocardial and epicardial source points to the simulated potentials at the electrode locations (9). A Wilson terminal defined the reference for measured and computed unipolar signals (10).

For inverse computation of the ventricular activation sequence, the target beats were selected with an automated signal processing algorithm as previously described (11). In brief, the model-based computation of the activation sequence of a single beat can be described as follows: for an assumed model-activation sequence, the ECG is simulated and compared with the measured ECG; the activation sequence is then systematically changed to minimize the difference between the simulated and the measured data. The optimization routine described in the study by Fischer et al. (9) was used to compute the activation sequence that

Table 1. Patient Characteristics

Patient #	Gender	Age (yrs)	Height (cm)	Weight (kg)	Ventricular Insertion of Accessory Pathway
1	F	25	163	45	LL
2	M	24	168	75	LPL
3	F	45	186	83	RL
4	M	34	171	57	LPL
5	F	33	165	67	LAL
6	M	20	178	64	RPS
7	M	24	178	60	LL

Data are presented as absolute values.
LAL = left anterolateral; LL = left lateral; LPL = left posterolateral; RL = right lateral; RPS = right posteroseptal.

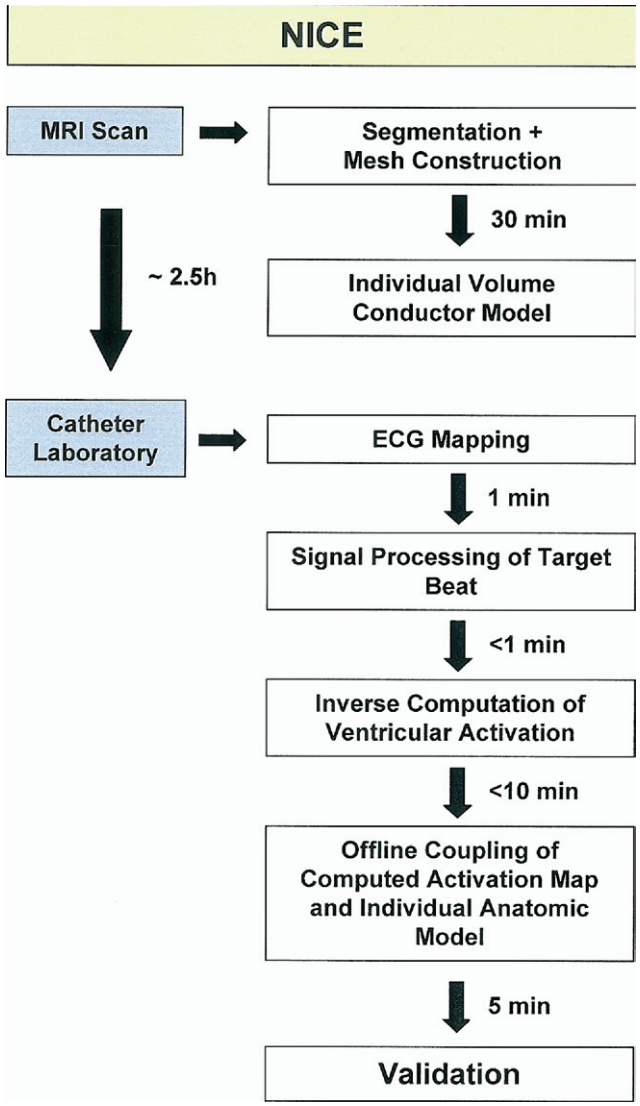

Figure 1. Noninvasive imaging of cardiac electrophysiology (NICE) workflow, including duration of the various procedural steps. ECG = electrocardiographic; MRI = magnetic resonance imaging.

best fits the measured data. The initial estimation of the activation sequence was computed by applying the critical point theorem (12). Because this imaging problem was ill-posed (i.e., the solution was sensitive to noise and model error), an additional regularization term of the Tikhonov second-order type was considered in the optimization process. This regularization imposes the constraint that neighboring source points have similar activation times (smooth activation pattern). The coupled regularization strategy was applied to solve the nonlinear optimization problem (9). The basic idea underlying coupled regularization is to use the starting vector obtained with the critical point theorem solely for optimization with the largest regularization parameter. When reducing the regularization parameter in each subsequent step, the previous step's solution is chosen as the new starting vector. This couples each regularization step with the previous one and reduces the sensitivity of the results with regard to the choice of regularization parameter. Details on the NICE method have been previously published (3,7,9,13).

Data acquisition. During electrophysiologic examination an intravenous bolus injection of adenosine (18 mg in patients >50 kg, 12 mg in others) was administered after placing a catheter in the right ventricular apex to provide backup pacing (at an interval of 1,500 ms). At the time of drug administration, ECG map recording was commenced and a segment of 30 s was recorded. Adenosine has a specific effect on the atrioventricular (AV) node, blocking the T-type calcium channels (responsible for depolarization in the AV node). Therefore, the accessory pathway remained the only input for ventricular activation, whereas under baseline conditions there were 2 activation inputs for ventricular activation: 1) the accessory pathway, and 2) the AV node. The short half-life of adenosine (approximately 1.5 s) caused only a few QRS complexes to show altered morphology due to the single ventricular input. This ECG pattern was termed "A" (adenosine) morphology in this study. The typical delta wave pattern under baseline conditions reflecting 2 ventricular inputs was termed "W" (WPW) morphology.

Signal processing. Automatic identification of the time interval of ventricular depolarization was performed as previously described (11). Briefly, an R-peak detector was used to identify each potential target beat. A direct signal classification method was applied to classify beats of "W" and "A" morphology, excluding beats of different morphology (ventricular ectopics, backup pacing) from the analysis. For both morphologies, a beat was exported to the NICE software (described in the preceding text) by clicking on the R-peak. Once a beat was selected for imaging, the start and the end of the global depolarization sequence were automatically determined from the rms trace of the mapping data. Within the time interval of depolarization the sampling rate was reduced to 500 Hz to permit fast computation of the activation map.

Radiofrequency ablation of accessory pathway. Ventricular activation of the accessory pathway was mapped during sinus rhythm with a 3D electroanatomic mapping system (CARTO). Left-sided accessory pathways were mapped with a multi-electrode catheter placed in the coronary sinus. However, ablation was performed at the endocardial ventricular insertion site of the accessory pathway with a retrograde approach via the aortic valve, aiming for the earliest ventricular activation as determined by coronary sinus mapping. Right-sided accessory pathways were mapped and ablated at the tricuspid annulus during sinus rhythm. After identifying the earliest ventricular activation, characterized as a hot spot in the CARTO map, radiofrequency energy was delivered in a temperature-controlled mode at a maximum temperature of 65°C and a power limit of 50 W. If we failed to interrupt conduction via the accessory pathway, radiofrequency energy delivery was stopped after a maximum of 10 s and the mapping continued. In the event that conduction via the accessory pathway was interrupted,

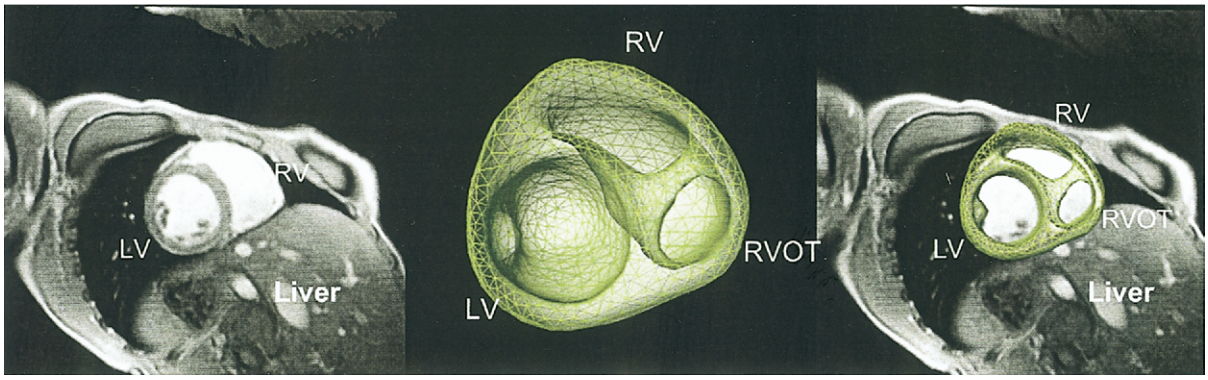

Figure 2. Ventricular surface model from a cardiac short-axis scan. The **left panel** shows a magnetic resonance imaging (MRI) slice (thickness 6 mm). The **middle panel** shows a triangulated and remeshed patient cardiac anatomy model with the left ventricle (LV), the right ventricle (RV), and the right ventricular outflow tract (RVOT). The **right panel** shows the fusion of MRI data and the cardiac anatomy model.

radiofrequency energy delivery was continued for a total of 60 s.

Validation of NICE-based activation time imaging. The reconstructed activation time maps of ventricular pre-excitation were validated with the catheter-based electro-anatomic data (CARTO) and anatomical markers. For quantitative analysis, the ablation site positions were digitized and coupled with the computer model as previously described (3,7). The last (successful) ablation site was used to calculate the spatial and temporal accuracy of NICE. The position error of the NICE-based activation mapping was defined as the distance between the site of earliest activation on the reconstructed NICE map and the successful ablation site on the CARTO map. The site of earliest activation was not necessarily located on the endocardium, because the NICE model also contains epicardial and basal source points. Data were obtained during baseline ("W" morphology) as well as during total AV block ("A" morphology).

Statistical analysis. Results are shown as mean values ± SD and are expressed as absolute values. Statistical analysis of the data was performed with SPSS 10.1 for Windows (SPSS Inc., Chicago, Illinois). The Student *t* test (unpaired) was used to evaluate the results, and a p value <0.05 was considered statistically significant.

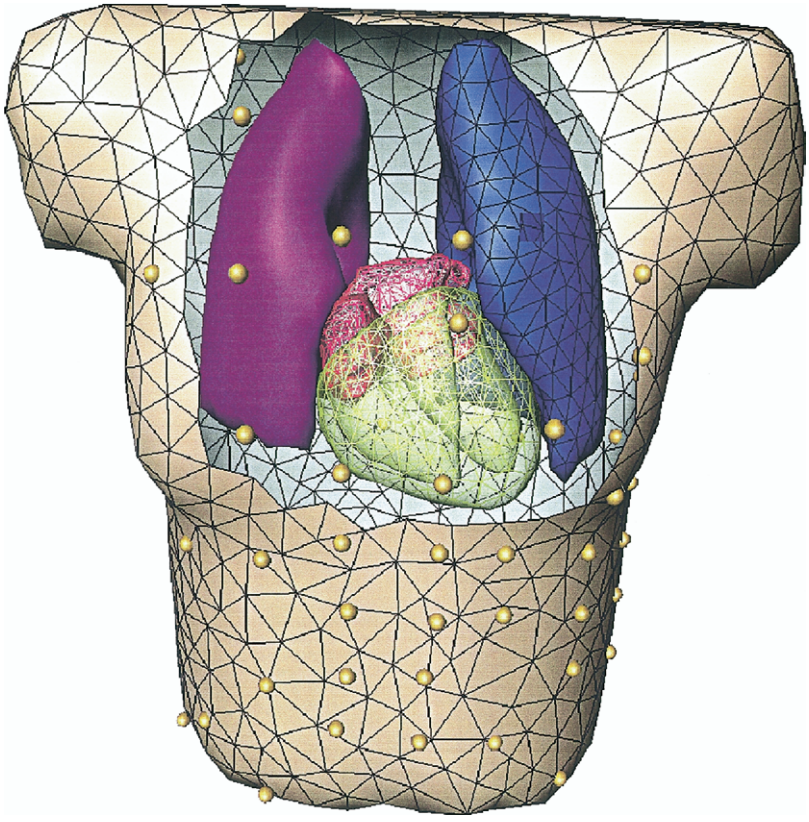

Figure 3. Patient-specific volume conductor model comprising chest, lungs, and cardiac compartments, including the particular blood masses. The electrode locations on the skin surface are indicated by **spherical markers**.

RESULTS

Acquisition of patient cardiac anatomy. Magnetic resonance imaging data were used to reconstruct a personal model of ventricular anatomy for all 7 patients with the boundary element method and linear triangular boundary elements. Resolution of the image data was 256 × 256 × 60 voxels. The mean number of triangles for the patient-specific ventricular mesh models was 1,317 ± 174. The mean edge length of the triangles was 10.0 mm. An example of a triangulated ventricular model obtained from MRI data is given in Figure 2. Figure 3 shows an example of the reconstructed volume conductor model.

NICE. The ventricular activation time sequence was calculated for each patient for the baseline QRS morphology ("W") as well as for the adenosine-induced AV block pattern ("A"), as shown in Figure 4. Figure 5 illustrates the automatic identification of the beginning and the end of the QRS complex calculated from the rms trace. The mean QRS interval duration for all patients was 125 ± 12 ms for "W" morphology and 153 ± 13 ms for "A" morphology ($p < 0.01$).

Electroanatomic coupling of CARTO and NICE data. A color-coded activation map was constructed for all 7 patients during baseline ("W") and AV block ("A"). The areas of first onset of ventricular activation are indicated in red and the areas of latest activation in blue. Isochrones are plotted in steps of 20 ms. As indicated in Figure 6, NICE-based identification of the accessory pathways was feasible for various ventricular insertion sites.

Position error of NICE-based activation time imaging. The mean distance from the successful ablation site (indicating the anatomical insertion site of the accessory pathway) to the surface of the ventricular model was 5 ± 3 mm. This parameter is an estimation of the error introduced by geometrically coupling the electroanatomic data with the NICE model. To quantify spatial dispersion of the ablation sites (n = 4.3 ± 3.7), the rms distance between the unsuccessful ablation sites and the site of successful treatment was determined (14 ± 5 mm). The points of earliest ventricular activation in the computed NICE sequences showed a strong concordance with the invasively determined successful ablation sites, namely a mean localization distance of 18.7 ± 5.8 mm during normal AV conduction and 18.7 ± 6.4 mm during adenosine-induced AV block. Data are shown in Table 2.

DISCUSSION

For the first time, noninvasive electrocardiographic imaging of ventricular pre-excitation was performed in the clinical setting of a catheter laboratory and validated with invasive electroanatomic mapping obtained from patients with WPW syndrome. Our results showed a strong concordance between the reconstructed activation sequences and the anatomical location of the accessory bundle insertion site as assessed by invasive electroanatomic mapping (CARTO). The ventricular activation maps reconstructed by NICE were obtained in a few minutes' computation time. Clinically important steps of signal processing, such as classification of QRS morphology, target beat selection, baseline

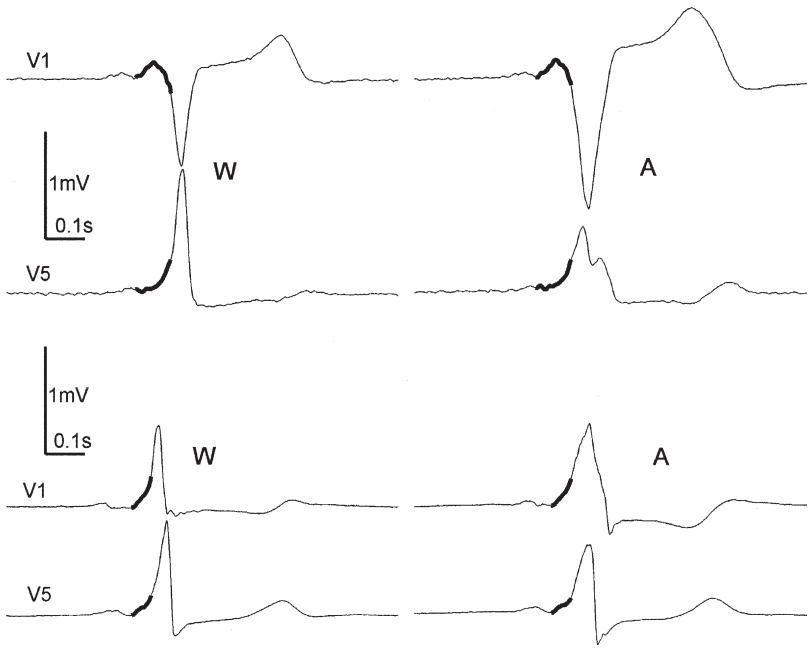

Figure 4. Wilson leads V_1 and V_5 for "W" (activation sequences during normal atrioventricular [AV] conduction) and "A" (activation sequences during adenosine-induced AV block) morphology in patients 3 **(upper panel)** and 5 **(lower panel)**. The first 90 ms (patient 3) and 60 ms (patient 5) of ventricular depolarization are marked with **bold lines**. Note that these initial depolarization upstrokes remain almost unchanged after adenosine administration in contrast to the remaining QRS and T-wave morphology.

JACC Vol. 48, No. 10, 2006
November 21, 2006:2045–52

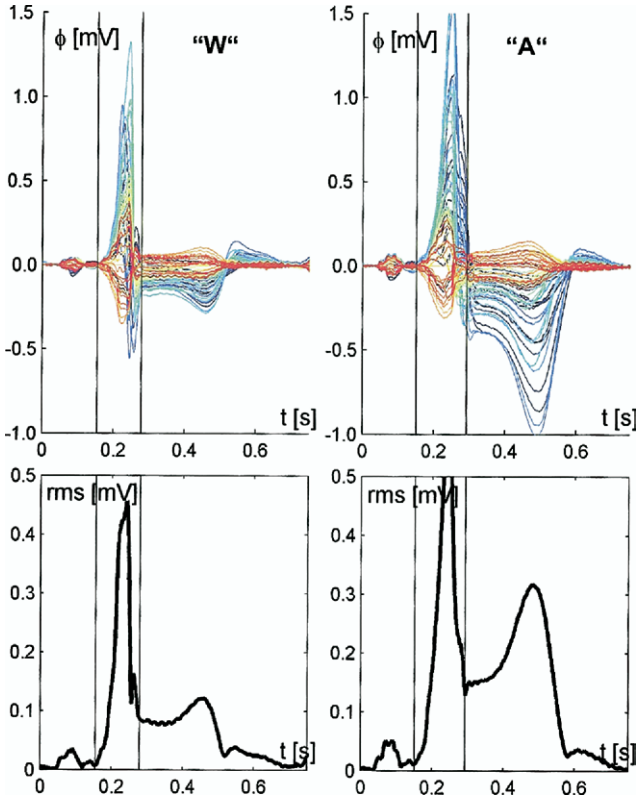

Figure 5. Butterfly plot **(upper panels)** and root mean square (rms) plot **(lower panels)** of the electrocardiographic mapping data recorded in patient 1. "W" (activation sequences during normal atrioventricular [AV] conduction) morphology is shown in the **left column** and "A" (activation sequences during adenosine-induced AV block) morphology in the **right column**. **Vertical calipers** mark the automatically detected beginning and end of the QRS complex.

correction, and identification of the interval of ventricular depolarization, were performed with a high level of automation. These findings and the sufficient localization accuracy of the ventricular insertion sites of the accessory pathways (as indicated by the similarity of ventricular activation sequences obtained with NICE and CARTO) during sinus rhythm as well as during adenosine-induced AV node block demonstrate that mapping of focal ventricular events is feasible.

NICE. Considerable efforts have been undertaken to solve the inverse problem of electrocardiography to localize and image cardiac activation sequences from body surface electrocardiograms (4–6,12,14). Previous studies have shown that the electrical excitation of the heart can be reconstructed by fusing data from surface ECG mapping and MRI (3,15). To date, clinical validation of these approaches in the setting of a catheter laboratory has been limited to case reports (3,4,7).

In this study, NICE was performed in patients with WPW syndrome during normal AV conduction as well as during adenosine-induced AV block. During baseline, ventricular activation resulted from input via the AV conduction and via the accessory pathway. After administering adenosine, a change in the ventricular activation pattern was observed. Ventricular activation resulted from a single input via the accessory pathway. For both sequences the origin of ventricular activation was imaged at the same location within the accuracy of current catheter treatment (rms distance). It should be emphasized that the transient "A" morphology activation sequences occurred only for a few beats, requiring a single-beat imaging method (11).

One might suspect that computation of the ventricular activation sequence during total AV block would result in better resolution of the NICE-based ventricular activation maps, because activation of the ventricular myocardium originates from one single input as compared with normal AV conduction. Interestingly, adenosine administration did not show any significant improvement in the resolution of the ventricular activation maps. This might be due to the fact that adenosine tends to increase the ventricular dispersion of depolarization and repolarization, as shown in Figure 5 (butterfly plot). This might reduce the imaging benefit of the single ventricular input during NICE.

Our results show the spatial and temporal resolution of the NICE data to be comparable to those of the CARTO data. The rms error between the various radiofrequency ablation points is approximately in the range of the mean distance error for the insertion point of the accessory pathway as obtained by NICE. In addition, conventional radiofrequency ablation catheters create lesions with an estimated size of 5 to 8 mm (16). Lesion size and dispersion of the radiofrequency ablation points, as indicated by the rms distance between the ablation sites, also limit the spatial precision and the accuracy of radiofrequency catheter ablation procedures.

Currently, the MRI segmentation and meshing procedure for reconstruction of the patient-specific anatomical model remains the most time-consuming part (approximately 30 min). In the catheter laboratory this information is available a few minutes after the ECG recording, enabling imaging of complex and unstable arrhythmias from single-beat ECG data. Ongoing development of imaging technologies (e.g., MRI and CT) will help facilitate cardiac modeling, even online in the catheter laboratory, during the coming years. Furthermore, we attempted to compute the ventricular activation sequences in a highly automated fashion as previously described (9,11). The algorithm used for automated QRS differentiation was able to distinguish the various QRS morphologies. This automation will be essential for further applications of NICE in clinical practice.

Clinical implications. Radiofrequency catheter ablation has become the standard treatment for patients with symptomatic WPW syndrome and has success rates of well over 90% (17). Noninvasive imaging of the ventricular activation sequence is of potential interest for catheter ablation treatment of patients with AV accessory pathways, because it might help identify the location of the accessory pathway as the target substrate within a few minutes. Therefore, NICE-based electroanatomic mapping might help decrease

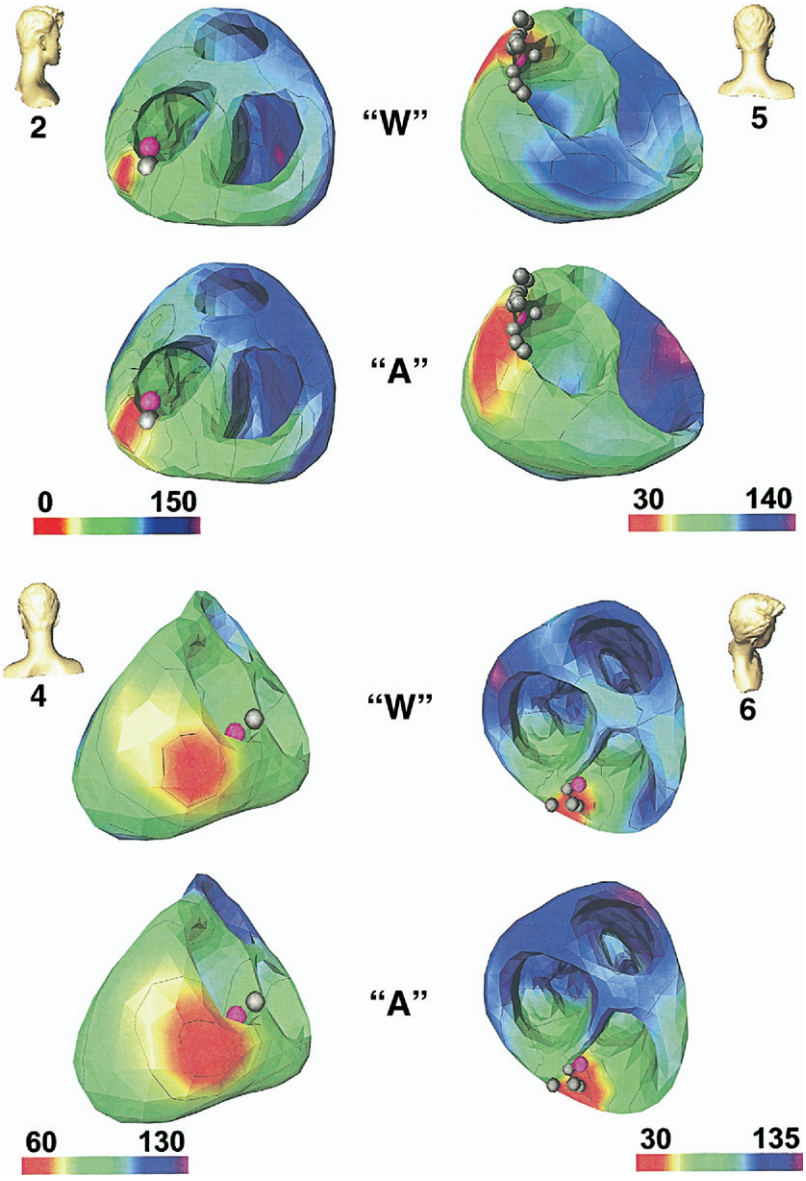

Figure 6. The location of earliest ventricular activation as computed by noninvasive imaging of cardiac electrophysiology is indicated in **red**. The ablation points are denoted by **grey markers**, and the location of successful ablation is given by a **purple marker**, indicating the ventricular insertion site of the accessory pathway. A left posterolateral accessory pathway was identified in patient 2, a left anterolateral accessory pathway in patient 5, a left posterolateral accessory pathway in patient 4, and a right posteroseptal accessory pathway in patient 6. **Upper panels** show activation sequences during normal atrioventricular (AV) conduction ("W"), **lower panels** show activation sequences during adenosine-induced AV block ("A"). **Head icons** indicate point of view. Isochrones are plotted in 20-ms intervals.

procedure duration, improve ablation outcome, and prevent complications, thanks to simultaneous visualization of cardiac anatomy and electrical excitation.

In contrast to other electroanatomic imaging techniques, NICE enables single-beat electroanatomic mapping, which is crucial for mapping unstable focal arrhythmias. Moreover, future developments of anatomical imaging will help further enhance the accuracy of NICE. Imaging of cardiac fiber orientation might help reduce model error by implementing cardiac anisotropy in the inverse algorithm. Furthermore, improvements in MRI and CT technologies might facilitate the fusion of anatomical images and NICE data and diminish coupling errors. Implementation of these developments in the NICE algorithm might help further increase the spatial and temporal resolution of this method.

Study limitations. The clinical validation of NICE is limited by the finite accuracy of the reference itself. Geometric coupling of the CARTO data and the MRI coordinate system was based on anatomical markers on the patient's chest, introducing an error of more than 5 mm (due to, e.g., breathing artifacts, markers outside the CARTO system's optimum measurement area). In future studies intrathoracic structures could be used as fiducial markers to further reduce position error.

Patient 3 showed a reduced accuracy of bundle localization. As compared with the other patients, this patient

JACC Vol. 48, No. 10, 2006
November 21, 2006:2045–52

Table 2. Position Error of NICE-Based Activation Time Imaging

#	Ablation Sites (n)	Distance HS-SAS (mm)	rms Distance (mm)	Distance NICE-SAS "W" (mm)	Distance NICE-SAS "A" (mm)
1	2	7.1	7.5	18.9	18.9
2	2	6.2	18.3	18.0	11.0
3	6	8.1	14.1	23.5	30.2
4	2	4.9	11.0	28.6	19.3
5	12	0.2	21.6	12.6	17.3
6	5	3.7	12.7	16.7	15.6
7	2	3.2	14.8	12.3	*
Mean ± SD	4.3 ± 3.7	5 ± 3	14 ± 5	18.7 ± 5.8	18.7 ± 6.4

*Adenosine was not administered because of a history of chronic obstructive lung disease.
"A" = adenosine-induced AV block (single ventricular input via accessory pathway; HS = heart surface of reconstructed individual cardiac model; NICE = noninvasive imaging of cardiac electrophysiology; SAS = successful ablation site; "W" = baseline (ventricular activation via atrioventricular [AV] conduction and accessory pathway).

showed no isoelectric segment before the QRS complex, indicating a fusion of atrial and ventricular signal components during early ventricular activation. However, the applied NICE model did not account for atrial signal components. This patient also showed a greater ventricular depolarization time interval for both morphologies ("W", 143 ms vs. 110 to 129 ms; "A", 179 ms vs. 139 to 159 ms) as compared with the other patients. This also implies that parts of ventricular repolarization contributed to the patient's ECG segment used for activation imaging. However, the applied NICE model did not include ventricular repolarization. Thus, the sum of these 2 model errors might be responsible for the increased localization error in this patient. Future improvements in the NICE algorithm, such as implementation of atrial components or cardiac repolarization, could help to overcome these problems. Studies of functional cardiac imaging using fusion of anatomical and ECG mapping are generally limited by the small number of study objects, owing to the complexity of data acquisition (3,4,6). Even the 7 patients included in this study are the lower limit for statistical evaluation. However, this study is the first attempt to systematically apply NICE in a cohort of patients undergoing treatment for a symptomatic arrhythmia. As a first step, this study indicates the feasibility of noninvasive imaging of ventricular pre-excitation. Further validation studies for various arrhythmogenic substrates are needed to improve the proposed method and establish NICE for clinical application in a catheter laboratory.

Conclusions. Our results indicate that NICE-based imaging of ventricular activation is feasible for single-beat data in the clinical setting of a catheter laboratory. Noninvasive imaging of cardiac electrophysiology might be used as a complementary noninvasive approach to localize the origin and help identify and understand the underlying mechanisms of cardiac arrhythmias.

Reprint requests and correspondence: Dr. Thomas Berger, Department of Internal Medicine, Division of Cardiology, Medical University Innsbruck, Anichstrasse 35, A–6020 Innsbruck, Austria. E-mail: t.berger@uibk.ac.at.

REFERENCES

1. Ben-Haim SA, Osadchy D, Schuster I, Gepstein L, Hayam G, Josephson ME. Nonfluoroscopic, in vivo navigation and mapping technology. Nat Med 1996;2:1393–5.
2. Dong J, Calkins H, Solomon SB, et al. Integrated electroanatomic mapping with three-dimensional computed tomographic images for real-time guided ablations. Circulation 2006;113:186–94.
3. Modre R, Tilg B, Fischer G, et al. Atrial noninvasive activation mapping of paced rhythm data. J Cardiovasc Electrophysiol 2003;14:712–9.
4. Ramanathan C, Ghanem RN, Jia P, Ryu K, Rudy Y. Noninvasive electrocardiographic imaging for cardiac electrophysiology and arrhythmia. Nat Med 2004;10:422–8.
5. Burnes JE, Taccardi B, Rudy Y. A noninvasive imaging modality for cardiac arrhythmias. Circulation 2000;102:2152–8.
6. Zhang X, Ramachandra I, Liu Z, Muneer B, Pogwizd SM, He B. Noninvasive three-dimensional electrocardiographic imaging of ventricular activation sequence. Am J Physiol Heart Circ Physiol 2005;289:H2724–32.
7. Tilg B, Fischer G, Modre R, et al. Model-based imaging of cardiac electrical excitation in humans. IEEE Trans Med Imaging 2002;21:1031–9.
8. Pfeifer B, Fischer G, Hanser F, et al. Atrial and ventricular myocardium extraction using model-based techniques. Methods Inf Med 2006;45:19–26.
9. Fischer G, Pfeifer B, Seger M, et al. Computationally efficient noninvasive cardiac activation time imaging. Methods Inf Med 2005;44:674–86.
10. Fischer G, Tilg B, Modre R, Hanser F, Messnarz B, Wach P. On modeling the Wilson terminal in the boundary and finite element method. IEEE Trans Biomed Eng 2002;49:217–24.
11. Fischer G, Hanser F, Pfeifer B, et al. A signal processing pipeline for noninvasive imaging of ventricular preexcitation. Methods Inf Med 2005;44:508–15.
12. Huiskamp G, Greensite F. A new method for myocardial activation imaging. IEEE Trans Biomed Eng 1997;44:433–46.
13. Greensite F. Demonstration of "discontinuities" in the time derivatives of body surface potentials, and their prospective role in noninvasive imaging of the ventricular surface activation map. IEEE Trans Biomed Eng 1993;40:1210–8.
14. Cheng LK, Bodley JM, Pullan AJ. Comparison of potential- and activation-based formulations for the inverse problem of electrocardiology. IEEE Trans Biomed Eng 2003;50:11–22.
15. Modre R, Tilg B, Fischer G, Wach P. Noninvasive myocardial activation time imaging: a novel inverse algorithm applied to clinical ECG mapping data. IEEE Trans Biomed Eng 2002;49:1153–61.
16. Simmons WN, Mackey S, He DS, Marcus FI. Comparison of gold versus platinum electrodes on myocardial lesion size using radiofrequency energy. Pacing Clin Electrophysiol 1996;19:398–402.
17. Schilling RJ. Which patient should be referred to an electrophysiologist: supraventricular tachycardia. Heart 2002;87:299–304.